Supplementary Information

SUPPLEMENTARY FIGURES

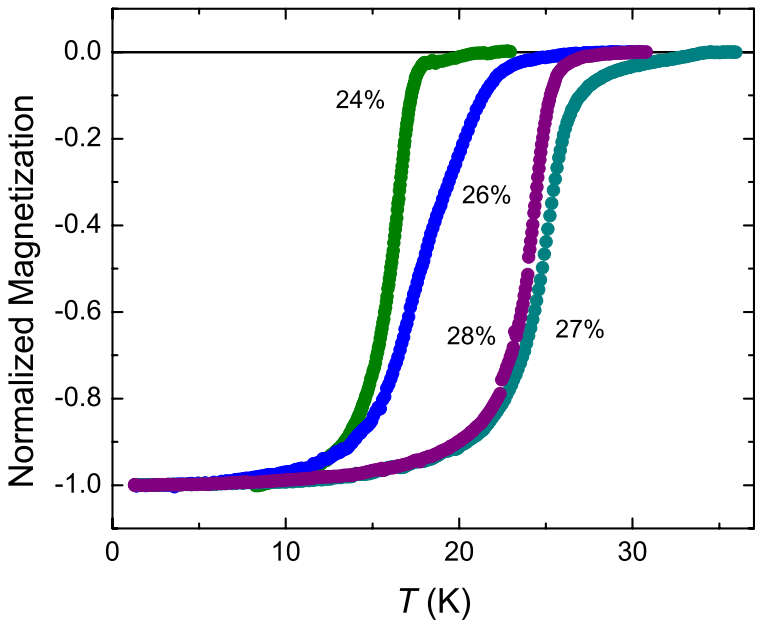

SUPPLEMENTARY FIGURE 1: DC magnetization for $Ba_{1-x}Na_xFe_2As_2$ (x = 0.24, 0.26, 0.27, and 0.28) in 0.02 Oe applied field.

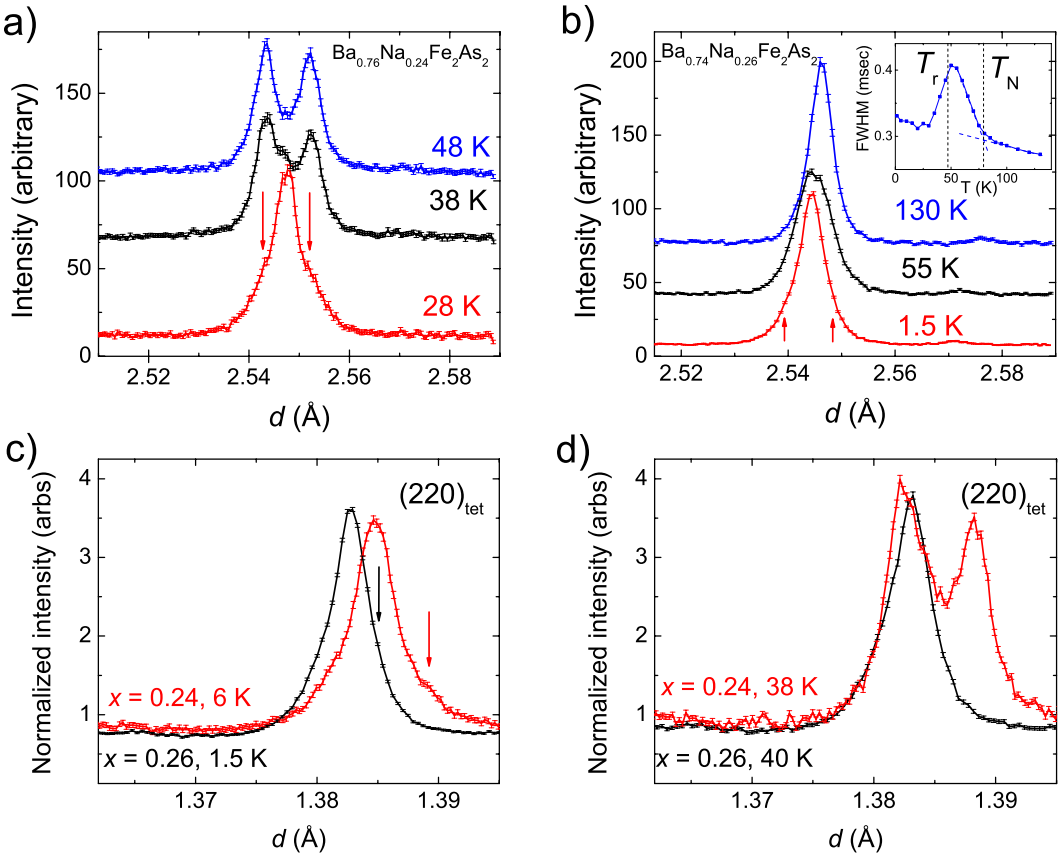

SUPPLEMENTARY FIGURE 2: (a) and (b): HRPD measurements of the (112) Bragg peak in $Ba_{1-x}Na_xFe_2As_2$ for a) $x = 0.24$ at $T = 28$ K, 38 K, and 48 K and b) $x = 0.26$ at 1.5 K, 55 K, and 130 K. Arrows mark the position of the Bragg peaks from the orthorhombic phase, which coexists with the tetragonal phase below the C_4 transition. Although the orthorhombic splitting cannot be seen by eye in the $x = 0.26$ sample, its onset is evident from the peak's full-width at half maximum (inset) and gives rise to shoulders at 1.5 K that are not present in the paramagnetic phase (130 K). (c) and (d): HRPD measurements of the (220) Bragg peak in $Ba_{1-x}Na_xFe_2As_2$ for $x = 0.24$ and 0.26 at c) low temperature and d) ~ 40 K. This comparison shows that there is little overlap between the the d-spacings of the residual orthorhombic phases in both samples. The error bars are derived from the square root of the raw detector counts.

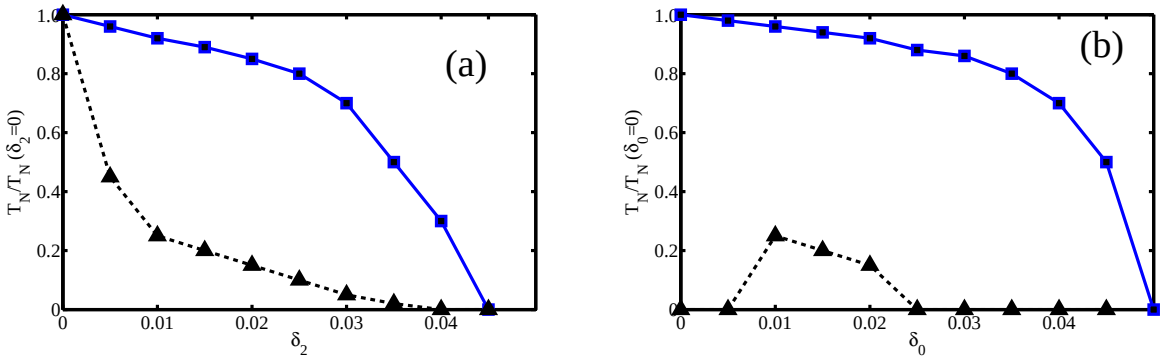

SUPPLEMENTARY FIGURE 3: Calculated magnetic phase diagram as a function of the ellipticity δ_2 at a finite mismatch between the electron and hole pockets, $\delta_0 = 0.01$ (a) and as a function of the mismatch δ_0 for the finite ellipticity $\delta_2 = 0.01$ (b). The parameter δ_0 increases with increasing doping. The squares denote the Néel temperature for the stripe phase. The triangles denote the temperature below which the C_4 phase wins over the stripe phase, although the two phases remain nearly degenerate in energy. The solid and dashed curves are guides to the eye. We used $U_{sdw} = 0.8$eV, $\epsilon_0 = 0.2$eV, and $m = 1eV$. In (b), the energies of the C_4 and the stripe phases are very close for all T, so C_4 phase may actually win at low T in a more generic model.

SUPPLEMENTARY NOTES

1. Sample Stoichiometry

Using the synthesis conditions described in the article's Methods section, we observed well-defined superconducting transitions (Supplementary Figure 1) in zero-field-cooled direct current (dc) magnetization measurements at 0.02 Oe. The $x = 0.24$, 0.27, and 0.28 samples show sharp transitions similar to those reported in Ref [1]. The $x = 0.26$ shows a somewhat broader transition although there is no evidence of compositional fluctuations from neutron powder diffraction. In measurements taken on the high resolution diffractometer, HRPD, the $x = 0.24$, 0.26, and 0.28 samples all have sharp Bragg peaks. It is possible that the width of the $x = 0.26$ transition results from the intrinsic coexistence of orthorhombic and tetragonal phases, which we discuss in the next section, but this needs further investigation. The Bragg peak widths of the $x = 0.27$ sample are slightly broader and the slight decrease in the magnetization of the $x = 0.27$ sample at 34 K suggests some compositional inhomogeneity in this sample, although the volume fraction would be too small to affect the neutron powder diffraction results.

We note that Aswartham *et al* [2] show measurements on a sample with a reported stoichiometry of $x = 0.25$, without seeing any thermodynamic anomalies associated with the C_4 transitions reported here. However, they report $T_N = 117$ K and $T_c = 9$ K, which is more consistent with $x \approx 0.18$ in the phase diagram of Avci *et al* [1], so their sample is unlikely to be in the narrow compositional range in which we observe the C_4 phase. However, as we mention in the Introduction, Hassinger *et al* [3] see transport anomalies in $Ba_{1-x}K_xFe_2As_2$ under pressure that they attribute to a new spin-density-wave (SDW) phase. These would be consistent with our own observations if pressure stabilizes the C_4 phase at lower hole-dopings, which is reasonable since pressure also suppresses SDW order [4].

2. Determination of the Phase Diagram

The temperature of the phase transition into the C_2 stripe phase, T_N, is determined both by the onset of the orthorhombic splitting of the tetragonal (112) peak and the intensity increase of $(\frac{1}{2}\frac{1}{2}l)$ magnetic Bragg peaks, where $l = 2n + 1$. As in the other compositions reported by Avci *et al* [1], both transitions are coincident at $x = 0.24$ and 0.26. However, the orthorhombic distortion becomes progressively weaker with increasing x, so the splitting is only seen by the increase in peak widths at $x = 0.26$ (see the inset of Supplementary Figure2b) and cannot be resolved at all at $x = 0.27$ and 0.28. However, the C_2 transition is still evident in the magnetic Bragg peak intensities, so these are used to determine T_N at higher doping. There is no evidence that the magnetic structure at $x = 0.27$ and 0.28 differs from the stripe SDW order seen at lower doping, so these samples are magnetically orthorhombic, even if the structural orthorhombicity is not measurable.

The diffractograms in Fig. 1 of the main article shows that the orthorhombic splitting apparently collapses at the C_4 transition in $x = 0.24$ and 0.26, producing a reentrant tetragonal phase. However, there is really a phase coexistence of the new tetragonal phase with a remnant orthorhombic phase, as illustrated by the transfer of peak intensity from the orthorhombic peaks to the tetragonal peaks shown in Supplementary Figure 2. The orthorhombic peaks persist with approximately the same splitting down to the lowest temperatures, as can be seen in the $x = 0.24$ sample at 28 K in Supplementary Figure 2(a) and the $x = 0.26$ sample at 1.5 K in Supplementary Figure 2(b). We estimate that approximately 40% of the sample remains orthorhombic at $x = 0.24$ and 20% at $x = 0.26$. The coexistence of both phases indicates that C_4 transition is first-order.

Since the orthorhombic splitting cannot be resolved at $x = 0.27$ and 0.28, the C_4 transition is most clearly seen in the rapid increase in the intensity of the $(\frac{1}{2}\frac{1}{2}1)$ peak seen in the WISH data. This peak is present in the C_2 phase, but becomes much stronger in the C_4 phase, reflecting a reorientation of the spins from the stripe phase. Therefore, we have labelled the transition T_r, the 'r' stands for reorientation. Although the peaks are too weak for a reliable Rietveld refinement of the magnetic structure, the signature of the spin reorientation is the same in all four samples so it is reasonable to assume that T_r represents the phase boundary from the C_2 phase into the C_4 phase over the entire range from $x = 0.24$ to 0.28. It is not possible to say whether the transition remains first-order in the higher-doped samples, since we cannot determine whether there is phase coexistence in these compounds.

There are two scenarios that can explain the phase coexistence below T_r in some of the samples. One possibility is that it is due to heterogeneous fluctuations in the local composition that straddle the phase line. However, if this were the case, we would expect the remnant C_2 peaks within the C_4 phase to have a similar d-spacings to samples on the low-doped side of the C_4 phase line, *i.e.*, $x < 0.24$. However, Supplementary Figure 2(a) and (b) shows that the residual C_2 shoulders are centered around the tetragonal peak and that there is a large and unequivocal difference between the location of these shoulders in the two samples. This is more clearly seen in Supplementary Figure 2(c)

and (d), where there is a significant difference between the shoulders in $x = 0.26$ and the orthorhombic peaks in $x = 0.24$. If the peak broadening in $x = 0.26$ at low T came from a fraction of the sample with $x \lesssim 0.24$ then the orthorhombic component would exhibit itself as satellite peaks shifted away from the tetragonal peak instead of shoulders surrounding it.

It is more likely that these samples are biphasic where two phases of equivalent composition coexist and the relative phase fractions are an independent parameter. This is plausible because it implies that the energy separation between ground states is very small, so that statistically both phases must be present. Incomplete transformation could be a kinetic effect—where the rate of cooling determines the relative phase fractions—or it could be indicative of slow dynamic fluctuations between orthorhombic and tetragonal symmetry.

SUPPLEMENTARY METHODS

Theory of the Reentrant C_4 Phase

The magnetic phase in most parent compounds of the iron-based superconductors is the stripe spin-density wave order with momentum either $\mathbf{Q_X} = (0, \pi)$ or $\mathbf{Q_Y} = (\pi, 0)$ in the unfolded Brillouin zone, in which there is one iron atom per unit cell [5, 6] (see Fig. 1(b) in the main manuscript). These two wavevectors connect the hole pockets at the center of the Brillouin zone and the electron pockets at the zone boundary, along the two orthogonal iron-iron bond directions. The stripe magnetic ordering breaks both $O(3)$ spin-rotational symmetry and C_4 lattice rotational symmetry (by selecting either $\mathbf{Q}_X$ or $\mathbf{Q}_Y$), and is often preceded by a "nematic" phase in which C_4 symmetry is broken, but $O(3)$ rotational symmetry remains unbroken.

In general, the geometry of iron pnictides allows more complex orders in which both $\mathbf{\Delta}_X$ and $\mathbf{\Delta}_Y$ are present. Previous analysis by two of us [7] have shown that near T_N, when Ginzburg-Landau theory is valid, the system definitely prefers a stripe order in which only the order parameter with $\mathbf{Q}_X$ or $\mathbf{Q}_Y$ is non-zero. Here we extend the previous analysis to lower T and study the magnetic order between $T = T_N$ and $T = 0$. Our results show that the phase diagram of the system is more complex than previously thought. In particular, we find that at some range of dopings, the system undergoes a first-order transition, upon lowering T, into a phase in which there is a two-component order parameter with equal magnitudes of the components with $\mathbf{Q}_X$ and $\mathbf{Q}_Y$, and the four-fold lattice rotational symmetry is restored (we label this phase as a C_4 phase). A similar result has been recently reported in Ref. [8]. The first order phase transition between the C_2 stripe and C_4 phases is consistent with the observed by neutron diffraction experiments reported in the main text.

We consider the minimal three-band model with the hole pocket Γ at the center of the Brillouin zone and two electron pockets X and Y at $\mathbf{Q}_X$ and $\mathbf{Q}_Y$, respectively. For simplicity, we consider parabolic dispersions with $\xi_{\Gamma,\mathbf{k}} = \varepsilon_0 - \frac{k^2}{2m} - \mu$, $\xi_{X,\mathbf{k}+\mathbf{Q_X}} = -\varepsilon_0 + \frac{k_x^2}{2m_x} + \frac{k_y^2}{2m_y} - \mu$, and $\xi_{Y,\mathbf{k}+\mathbf{Q_Y}} = -\varepsilon_0 + \frac{k_x^2}{2m_y} + \frac{k_y^2}{2m_x} - \mu$, where m_i denotes the band masses, ε_0 is the offset energy, and μ is the chemical potential. Near the Fermi energy and for small ellipticity, the dispersions can be approximated by $\xi_{\Gamma,\mathbf{k}} = -\xi$, $\xi_{X,\mathbf{k}+\mathbf{Q_X}} = \xi - \delta_0 + \delta_2 \cos 2\theta$, $\xi_{Y,\mathbf{k}+\mathbf{Q_Y}} = \xi - \delta_0 - \delta_2 \cos 2\theta$, with $\delta_0 = 2\mu$, $\delta_2 = \varepsilon_0 m(m_x - m_y)/(2m_x m_y)$, and $\theta = \tan^{-1} k_y/k_x$ [9] .

Electrons with spin α of the band i are created by the operators $c^\dagger_{i,\mathbf{k}\alpha}$, and free-fermion part of the Hamiltonian has the form

$$\mathcal{H}_0 = \sum_{i,\mathbf{k}} \xi_{i,\mathbf{k}} c^\dagger_{i,\mathbf{k}\alpha} c_{i,\mathbf{k}\alpha} \tag{1}$$

Here the summation over repeated spin indices is assumed, and we shift the momenta of the fermions near the X and Y Fermi pockets by $\mathbf{Q}_X$ and $\mathbf{Q}_Y$, respectively, *i.e.*, write $\xi_{X,\mathbf{k}+\mathbf{Q_Y}} = \xi_{X,\mathbf{k}}$, $\xi_{Y,\mathbf{k}+\mathbf{Q_Y}} = \xi_{Y,\mathbf{k}}$.

To shorten presentation, we restrict the interacting part of Hamiltonian to the interaction in the spin channel with momenta near $\mathbf{Q}_X$ and $\mathbf{Q}_Y$, i.e., to

$$\mathcal{H}_\mathrm{int} = -\frac{1}{2} U_\mathrm{spin} \sum_{i,\mathbf{q}} \mathbf{s}_{i,\mathbf{q}} \cdot \mathbf{s}_{i,-\mathbf{q}} \tag{2}$$

where $\mathbf{s}_{i,\mathbf{q}} = \sum_k c^\dagger_{\Gamma,\mathbf{k}+\mathbf{q}\alpha} \boldsymbol{\sigma}_{\alpha\beta} c_{i,\mathbf{k}\beta}$ is the electronic spin operator, and $\boldsymbol{\sigma}_{\alpha\beta}$ are Pauli matrices. The coupling U_spin is the sum of density-density and pair-hopping interactions between hole and electron states ($U_\mathrm{spin} = U_1 + U_3$ in the notation of Ref. [10]), where

$$U_1 c^\dagger_{\Gamma,\alpha} c_{\Gamma,\alpha} c^\dagger_{X,\beta} c_{X,\beta} \;=\; -\frac{U_1}{2} c^\dagger_{\Gamma,\alpha} \boldsymbol{\sigma}_{\alpha\beta} c_{X,\beta} \cdot c^\dagger_{X,\gamma} \boldsymbol{\sigma}_{\gamma\delta} c_{\Gamma,\delta}$$

$$
\begin{aligned}
& +(\cdots) \\
U_3 c^\dagger_{\Gamma,\alpha} c_{X,\alpha} c^\dagger_{\Gamma,\beta} c_{X,\beta} \;&=\; -\frac{U_3}{2} c^\dagger_{\Gamma,\alpha} \boldsymbol{\sigma}_{\alpha\beta} c_{X,\beta} \cdot c^\dagger_{\Gamma,\gamma} \boldsymbol{\sigma}_{\gamma\delta} c_{X,\delta} \\
& +(\cdots)
\end{aligned} \tag{3}
$$

and the dots stand for the terms with $\delta_{\alpha,\beta}\delta_{\gamma,\delta}$, which only contribute to the CDW channel. The couplings U_1 and U_3 do depend on the angle along the electron pockets [11], but for our purposes this dependence may be neglected, i.e., $U_{\rm spin}$ can be approximated by a constant. Once $U_{\rm spin}$ exceeds some critical value (which gets larger when δ_0 and δ_2 increase), the static magnetic susceptibility diverges at $(0,\pi)$ and $(\pi,0)$, and the system develops long-range magnetic order.

To understand what kind of magnetic order wins below $T_{\rm N}$ we introduce the two spin fields $\boldsymbol{\Delta}_{(X,Y)} = U_{spin} \sum_{\mathbf{k}} c^\dagger_{\Gamma,\mathbf{k}\alpha} \boldsymbol{\sigma}_{\alpha\beta} c_{(X,Y),\mathbf{k}\beta}$. We apply Hubbard-Stratonovich transformation, integrate out fermions, obtain the action $S[\boldsymbol{\Delta}_X, \boldsymbol{\Delta}_Y]$ in terms of $\boldsymbol{\Delta}_X$ and $\boldsymbol{\Delta}_Y$, use saddle-point approximation $\partial S/\partial \boldsymbol{\Delta}_i = 0$, and solve a set of coupled saddle-point equations for $\boldsymbol{\Delta}_X$ and $\boldsymbol{\Delta}_Y$ A straightforward way to perform this calculation is to introduce the 6-dimensional Nambu operator:

$$
\Psi^\dagger_{\mathbf{k}} = \left(\begin{array}{cccccc} c^\dagger_{\Gamma,\mathbf{k}\uparrow} & c^\dagger_{\Gamma,\mathbf{k}\downarrow} & c^\dagger_{X,\mathbf{k}\uparrow} & c^\dagger_{X,\mathbf{k}\downarrow} & c^\dagger_{Y,\mathbf{k}\uparrow} & c^\dagger_{Y,\mathbf{k}\downarrow} \end{array} \right) \tag{4}
$$

Applying the Hubbard-Stratonovich transformation and evaluating the products of the Pauli matrices, we obtain the partition function in the form [12, 13]:

$$
Z = \int d\Delta_i d\Psi \mathrm{e}^{-S[\Psi,\Delta_i]} \tag{5}
$$

with the action

$$
S\left[\Psi,\Delta_i\right] = -\int_k \Psi^\dagger_k \mathcal{G}^{-1}_k \Psi_k + \frac{2}{U_{\rm spin}} \int_x \left(\Delta^2_X + \Delta^2_Y\right) \tag{6}
$$

Here $\Delta_i = |\boldsymbol{\Delta}_i|$, and the Green's function $\mathcal{G}^{-1}_k$ is given by:

$$
\mathcal{G}^{-1}_k = \mathcal{G}^{-1}_{0,k} - \mathcal{V} \tag{7}
$$

where the free-fermion term is

$$
\mathcal{G}_{0,k} = \left(\begin{array}{ccc} \hat{G}_{\Gamma,k} & 0 & 0 \\ 0 & \hat{G}_{X,k} & 0 \\ 0 & 0 & \hat{G}_{Y,k} \end{array} \right) \tag{8}
$$

and the interaction term is

$$
\mathcal{V} = \left(\begin{array}{ccc} 0 & -\hat{\Delta}_X & -\hat{\Delta}_Y \\ -\hat{\Delta}_X & 0 & 0 \\ -\hat{\Delta}_Y & 0 & 0 \end{array} \right) \tag{9}
$$

Here we introduced the 2×2 matrices $\hat{G}_{i,k} = G_{i,k}\mathbb{I}$ and $\hat{\Delta}_i = \boldsymbol{\Delta}_i \cdot \boldsymbol{\sigma}$, where $\mathbb{I}$ is the identity matrix. The functions $G^{-1}_{i,k} = i\nu_n - \xi_{i,\mathbf{k}}$ are the non-interacting single-particle Green's functions for Γ, Y, and X fermions.

It is now straightforward to integrate out the fermions, since the action is quadratic in them, and obtain the effective magnetic action:

$$
S_{\rm eff}\left[\boldsymbol{\Delta}_X, \boldsymbol{\Delta}_Y\right] = -\mathrm{Tr} \ln\left(1 - \mathcal{G}_{0,k}\mathcal{V}\right) + \frac{2}{u_{\rm spin}} \int_x \left(\Delta^2_X + \Delta^2_Y\right) \tag{10}
$$

Here $\mathrm{Tr}\left(\cdots\right)$ refers to the sum over momentum, frequency and Nambu indices. In contrast to the previous studies [7, 13], we do not perform a series expansion in powers of Δ^2_i but analyze the full non-linear saddle-point (mean-field) solutions $\frac{\delta S}{\delta \Delta_i} = 0$ for the two cases: (i) a C_2 stripe phase, in which we set $\Delta_X \neq 0$, $\Delta_Y = 0$ and (ii) a C_4 phase in which we set $\Delta_X = \Delta_Y = \Delta$ For the case (i), the mean-field equation has the form

$$
1 = 2U_{spin}\Delta_X \sum_{\mathbf{k},i\nu_n} \frac{1}{\Delta^2_X - G^{-1}_{\Gamma,k} G^{-1}_{X,k}} \tag{11}
$$

while for the case (ii) we have

$$1 = 2U_{spin}\Delta \sum_{\mathbf{k},i\nu_n} \frac{1}{\Delta^2 - G^{-1}_{\Gamma,k}G^{-1}_{X,k} + \Delta^2 G^{-1}_{X,k}G_{Y,k}} \tag{12}$$

In both cases the sum over Matsubara frequencies can be evaluated exactly. For stripe magnetic order, the mean-field equation becomes

$$1 = -2U_{spin}\Delta_X \sum_{\mathbf{k}} \frac{f\left(E_{1\mathbf{k}}\right) - f\left(E_{2\mathbf{k}}\right)}{E_{1\mathbf{k}} - E_{2\mathbf{k}}} \tag{13}$$

where $E_{1,2\mathbf{k}} = \frac{1}{2}\left(\xi_{\Gamma,\mathbf{k}} + \xi_{X,\mathbf{k}+\mathbf{Q_X}} \pm \sqrt{\left(\xi_{\Gamma,\mathbf{k}} - \xi_{X,\mathbf{k}+\mathbf{Q_X}}\right)^2 + 4\Delta_X^2}\right)$. For the C_4 phase, we obtain

$$\begin{aligned} 1 = -2U_{spin}\Delta \sum_{\mathbf{k}} \quad & \left[\frac{\left(E_{11\mathbf{k}} - \xi_{X,\mathbf{k}+\mathbf{Q_Y}}\right) f\left(E_{11\mathbf{k}}\right)}{\left(E_{11\mathbf{k}} - E_{22\mathbf{k}}\right)\left(E_{11\mathbf{k}} - E_{33\mathbf{k}}\right)} - \frac{\left(E_{22\mathbf{k}} - \xi_{X,\mathbf{k}+\mathbf{Q_Y}}\right) f\left(E_{22\mathbf{k}}\right)}{\left(E_{11\mathbf{k}} - E_{22\mathbf{k}}\right)\left(E_{22\mathbf{k}} - E_{33\mathbf{k}}\right)}\right. \\ & \left. + \frac{\left(E_{33\mathbf{k}} - \xi_{X,\mathbf{k}+\mathbf{Q_Y}}\right) f\left(E_{33\mathbf{k}}\right)}{\left(E_{11\mathbf{k}} - E_{33\mathbf{k}}\right)\left(E_{22\mathbf{k}} - E_{33\mathbf{k}}\right)}\right] \end{aligned} \tag{14}$$

where the energies E_{ii} $(i = 1-3)$ are the three solutions of the cubic equation $\Delta^2(\omega - \xi_{X,\mathbf{k}+\mathbf{Q_X}}) + \Delta^2(\omega - \xi_{Y,\mathbf{k}+\mathbf{Q_Y}}) - (\omega - \xi_{\Gamma,\mathbf{k}})(\omega - \xi_{X,\mathbf{k}+\mathbf{Q_X}})(\omega - \xi_{Y,\mathbf{k}+\mathbf{Q_Y}}) = 0$

We solved these equations numerically together with the equation for the chemical potential, for different values of the chemical potential mismatch δ_0 and ellipticity parameter δ_2. Like in previous analysis [7, 12], we find that the actions for C_2 and C_4 phases are degenerate at zero ellipticity and for equal sizes of the electron and hole pockets ($\delta_0 = \delta_2 = 0$). Once ellipticity becomes non-zero, the C_2 wins near the Néel temperature. Within the Ginzburg-Landau expansion to order $\Delta^4_{X,Y}$, the lower free energy of the C_2 phase is the consequence of the fact that the ellipticity generates the term $C|\vec{\Delta_X}|^2|\vec{\Delta_Y}|^2$ with positive coefficient C, which increases the energy of the C_4 phase but does not affect C_2 phase. Going beyond Ginzburg-Landau approximation, we found that for small enough ellipticity, the solution of Eq. (14) re-emerges below some $T < T_N$ and, below this T, C_4 phase becomes a local minimum. Furthermore, in some range of Δ_2, at even lower $T < T_{\rm r}$, the free energy of the C_4 phase becomes slightly smaller than that of the C_2 phase, i.e., the system undergoes a first-order transition from C_2 to C_4 magnetic phase, and lattice C_4 symmetry gets restored.

At $\delta_0 = 0$ the region of δ_2 where C_4 phase wins is exponentially small. However, at a finite δ_0, this region widens up. We show the results for a particular δ_0 in Supplementary Figure 3(a) and for a given ellipticity as a function of δ_0 in Supplementary Figure 3(b). A non-zero δ_0 means that the sizes of electron and hole pockets are non-equal, i.e., that there is a finite amount of doping. The implication of this result is that, at a finite doping, as the temperature is lowered, the system first orders into a stripe C_2 phase in which four-fold lattice rotational symmetry is broken (X and Y directions become non-equivalent), and then, at a lower T, it undergoes a first order transition into the C_4 phase in which four-fold lattice rotational symmetry is restored. This is consistent with our experiment.

SUPPLEMENTARY REFERENCES

[1] S. Avci *et al.*, Phys. Rev. B **88**, 094510 (2013).
[2] S. Aswartham *et al.*, Phys. Rev. B **85**, 224520 (2012).
[3] E. Hassinger*et al.*, Phys. Rev. B **86**, 140502 (2012).
[4] E. Colombier*et al.*, Phys. Rev. B **79**, 224518 (2009).
[5] T. Yildirim, Phys. Rev. Lett. **101**, 057010 (2008).
[6] F. Ma, Z.-Y. Lu, and T. Xiang, Phys. Rev. B **78**, 224517 (2008).
[7] I. Eremin and A. V. Chubukov, Phys. Rev. B **81**, 024511 (2010).
[8] J. Kang and Z. Tešanović, Proceedings of the March meeting of the American Physical Society, 2013.
[9] A B Vorontsov, M G Vavilov, and Andrey V Chubukov, Phys. Rev. B **81**, 174538 (2010).
[10] A. V. Chubukov, D. V. Efremov, and I. Eremin, Phys. Rev. B **78**, 134512 (2008).
[11] Ying Ran, Fa Wang, Hui Zhai, Ashvin Vishwanath, and Dung-Hai Lee, Phys. Rev. B **79**, 014505 (2009).
[12] R. M. Fernandes and J. Schmalian Phys. Rev. B **82**, 014521 (2010).
[13] R.M. Fernandes, A.V. Chubukov, J. Knolle, I. Eremin, and J. Schmalian, Phys. Rev. B **85**, 024534 (2012)